Magnetic fatigue: Effect of seismic-related loading on magnetic and structural behavior of magnetite

Boris Reznik[1], Agnes Kontny[2], and Frank R. Schilling[1]

[1]Karlsruhe Institute of Technology
[2]KIT

November 23, 2022

Abstract

Powders of multidomain magnetite were subjected to fatigue, cyclic loading at ambient conditions between 30 and 500°C using a dynamical mechanical analysis system. The uniaxial static force of 6 MPa was modulated with 3 MPa using 1, 10 and 100 Hz frequencies. Microstructural analysis was performed by a combination of X-ray diffraction analysis with optical microscopy. Magnetic properties were studied by low-temperature magnetic susceptibility across the Verwey transition and hysteresis behavior measured at room temperature. Irreversible microstructures and magnetic signatures indicate the onset of magnetic fatigue in magnetite. The increasing mechanical losses, are proportional to the growing loading frequency and correlate with decreasing coherent crystallite size and lattice parameters in magnetite as well as with its lattice distortion. Hematite at grain boundaries of crashed magnetite is documented by microscopy, however, magnetic analysis indicates that magnetite is still the main magnetic carrier in the fatigue-loaded samples and therefore, the changes in magnetic properties are dominantly related to magnetic fatigue. The decay of magnetic susceptibility above is independent of the occurrence of hematite but is more sensitive to lattice strain and reduction of magnetic domains. The refinement of magnetic domains is also demonstrated by the evolution of hysteresis parameters and FORC diagrams, both indicating multidomain to pseudo-single domain transition. As the applied loading frequencies are similar to those observed during earthquake propagation or volcano eruption, it is therefore discussed how the acquired signatures of magnetic fatigue can be used as proxies of natural seismic-related loadings.

Magnetic fatigue: Effect of seismic-related loading on magnetic and structural behavior of magnetite

B. Reznik, A. Kontny and F. Schilling.

Karlsruhe Institute of Technology, Institute of Applied Geosciences, Karlsruhe, Germany.

E-mail:boris.reznik@kit.edu

Abstract

Powders of multidomain magnetite were subjected to fatigue, cyclic loading at ambient conditions between 30 and 500°C using a dynamical mechanical analysis system. The uniaxial static force of 6 MPa was modulated with 3 MPa using 1, 10 and 100 Hz frequencies. Microstructural analysis was performed by a combination of X-ray diffraction analysis with optical microscopy. Magnetic properties were studied by low-temperature magnetic susceptibility across the Verwey transition (Tv) and hysteresis behavior measured at room temperature. Irreversible microstructures and magnetic signatures indicate the onset of magnetic fatigue in magnetite. The increasing mechanical losses, $tan\ \delta$ are proportional to the growing loading frequency and correlate with decreasing coherent crystallite size and lattice parameters in magnetite as well as with its lattice distortion. Hematite at grain boundaries of crashed magnetite is documented by microscopy, however, magnetic analysis indicates that magnetite is still the main magnetic carrier in the fatigue-loaded samples and therefore, the changes in magnetic properties are dominantly related to magnetic fatigue. The decay of magnetic susceptibility above Tv is independent of the occurrence of hematite but is more sensitive to lattice strain and reduction of magnetic domains. The refinement of magnetic domains is also demonstrated by the evolution of hysteresis parameters and FORC diagrams, both indicating multidomain to pseudo-single domain transition. As the applied loading frequencies are similar to those observed during earthquake propagation or volcano eruption, it is therefore discussed how the acquired signatures of magnetic fatigue can be used as proxies of natural seismic-related loadings.

1. Introduction

Among diverse petrographic tools, magnetic methods allow a quick access to strain identification in deformed rocks (Nagata 1961, Nagata & Kinoshita 1964). Because magnetite is by far the most common magnetic mineral in crustal rocks, understanding of the relationship between applied loading conditions and magnetic behavior of magnetite or magnetite-bearing rocks is fundamental. Commonly, the magnetic response has been investigated in relation to static loading imitating tectonic-induced deformation. Magnetic properties such as bulk magnetic susceptibility (Till *et al.* 2012), characteristic Verwey transition (Carporzen and Gilder 2010) as well as hysteresis behavior (Volk & Feinberg 2019) are frequently used as fingerprints of strains localized in deformed rocks.

Rocks can be fractured not only under static stresses but also due to repeated loading and unloading, so-called fatigue loading (e.g. Cerfontaine & Collin 2018). Under such cyclic loading, rock fails at stresses well below the failure stress or yield stress limit observed under monotonic loading. For example, Liu et al. (2014) showed that intact rocks failed between 24 to 80 percent of its static strength. Cyclic loading phenomena can be either human-induced (e.g. drilling processes, oil and gas storage) or environmental-induced by earthquakes, volcanic hazards or even freeze-thaw cycles (e.g. in tunnels). Gomberg and Johnson (Gomberg & Johnson 2005) assumed that aftershocks of earthquakes are dynamically triggered and suggested that the dynamic elastic nonlinear behavior of cyclic loading observed in the laboratory is an analogue for the earthquake failure mechanism in view of the underlying physics. One explanation of the weakening effect under cyclic loading conditions is an increasing number of broken inter-particle bonds (e.g. Braunagel & Griffith 2019).

The types of seismic events can be schematically represented as function of loading frequency (Figure 1) influencing rock deformation degree and the accumulated strains or produced hazards. Consequently, laboratory experiments under controlled conditions, mimicking the natural deformation settings and revealing response of magnetic properties of rocks to applied cyclic/fatigue stresses is of special fundamental interest (see e.g. review by Cerfontaine and Collin 2017). However, documentation of the influence of fatigue loading on the fundamental magnetic properties of rocks or its magnetic carriers is sparse. Martin et al. (1978) studied the effect of static loading-unloading cyclic compression on the magnetic susceptibility of diabase. The compressions were conducted at room temperature and pressures up to 200 MPa. Interestingly, the change in susceptibility was explicitly related to differential stress and was found independent of confining pressure and the number of static loading-unloading cycles.
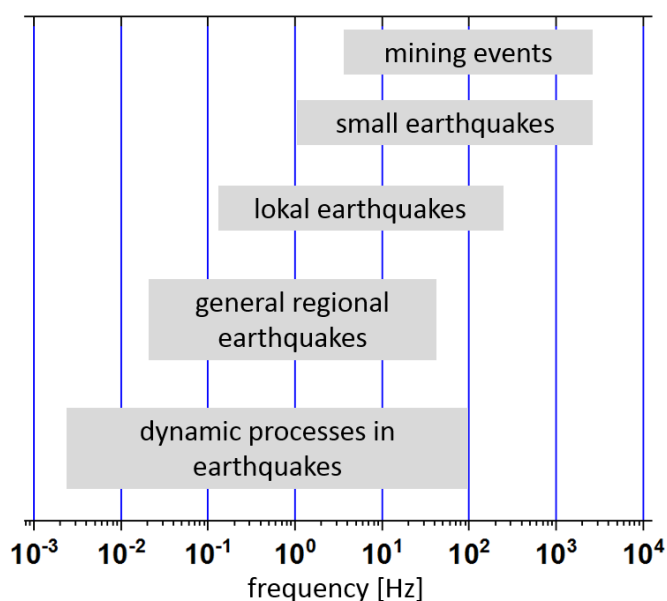

Fig. 1 Relevant frequencies during seismic events (modified from www.GeoSig.com).

Therefore, the main question of the present study is how magnetic properties of rocks respond to fatigue, cyclic loading. For our cyclic loading experiments of a magnetite powder we used the dynamical mechanical analysis DMA, which was recently successful used for the analysis of inelastic response of minerals to alternating loading (e.g. Harrison et al. 2004, Peng & Redfern 2013, Klumbach & Schilling 2013). Here, we report a non-linear relationship between the fatigue-induced degradation in magnetic behavior of magnetite, called magnetic fatigue, and the loading frequency. While loading experiments were carried out at ambient atmosphere, the variations in magnetic properties are not only related to magnetic fatigue but also to magnetite partial transformation into hematite.

2. Experimental methods

2.1 Material

The material used for this study was a magnetite-rich powder obtained from a banded iron ore (Sydvaranger mine Finnmark, Norway) containing about 80% of magnetite (further description see in Reznik et al. 2016). The magnetite from this ore has a stoichiometric composition of Fe_3O_4 and is mostly composed of multidomain (MD) grains. Beside magnetite, the ore also contains about 18 wt. % quartz and 2 wt. % of minor components including amphibole, biotite and pyrite. The investigated magnetite powder was extracted from the initial ore by repeated manual gentle crushing, screening and following multi-step manual magnetic separation until a homogeneously dark, powder appeared. Additionally, for magnetic measurements, binary mixtures of magnetite and hematite were prepared. For this purpose, magnetite powders extracted from the iron ore were mixed with a synthetic hematite powder supplied by Sigma Aldrich (LOT# MKCJ3303). To obtain a relatively large amount of magnetite powder, manually fractured chips of the iron ore were further dispersed in an achate mill for 5 minutes. After repeated manual screening and magnetic separation steps, a dark magnetite powder was extracted.

2.2 Cyclic compression experiments

In the case of an elastic body, the energy, which is necessary to deform a specimen is stored during loading and completely released to restore the initial body shape, as soon as stress is withdrawn. This relationship between stress σ and strain ε is described by the Hook's Law, introducing the Young's modulus E:

$$\sigma = E\,\varepsilon \tag{1}$$

During a cyclic compression loading, the static applied force Fs is superimposed with a modulated force Fd (Figure 2a). Therefore, the behavior of combined material properties are described by the dynamic Young's modulus E^*, consisting of the storage modulus E' and the dissipation modulus E'':

$$E^*(\omega) = E'(\omega) + iE''(\omega) \tag{2}$$

The angle δ between the complex modulus and the storage modulus again equals the phase lag between stress and strain:

$$\tan\delta = E''(\omega) \,/\, E'(\omega) \tag{3}$$

and is equivalent to the mechanical loss or internal friction in the material (Klumbach & Schilling 2013, Peng & Redfern 2013).

Figure 2b illustrates that in the case of falling ball the mechanical losses are equal to the conservation of inelastic energy, E'' (Saba *et al.* 2016). Similarly, the loading energy during cyclic loading is entirely dissipated, which means it is transformed into plastic deformation and heat. Using a DMA system, the frequency-dependent amplitudes of stresses and strains were recorded and the phase difference δ is used as a measure of inelastic losses (Figure 2c).

Our cyclic loading compressions were carried out using a GABO Eplexor DMA system described in detail elsewhere (Klumbach & Schilling 2013). Magnetite powders were cyclic compressed in a round shaped (5 mm diameter) uniaxial compression cell with a static force of 50 N applied by the punch (Figure 2d). The resulting static pressure in the mini cell was about 6 MPa. The modulating dynamic force of 25 N (3 MPa) was applied during 40 cycles using different fixed loading frequencies of 1, 10 and 100 Hz. The loading was carried out in air between 30 and 500°C with a 1°C step increment and a 2°C/min heating rate.

The selected temperature maximum and pressure correspond to the diffusion creep field of plastic deformation in magnetite (Till & Moskowitz 2013) while the selected temperature range corresponds to magnetite oxidation.
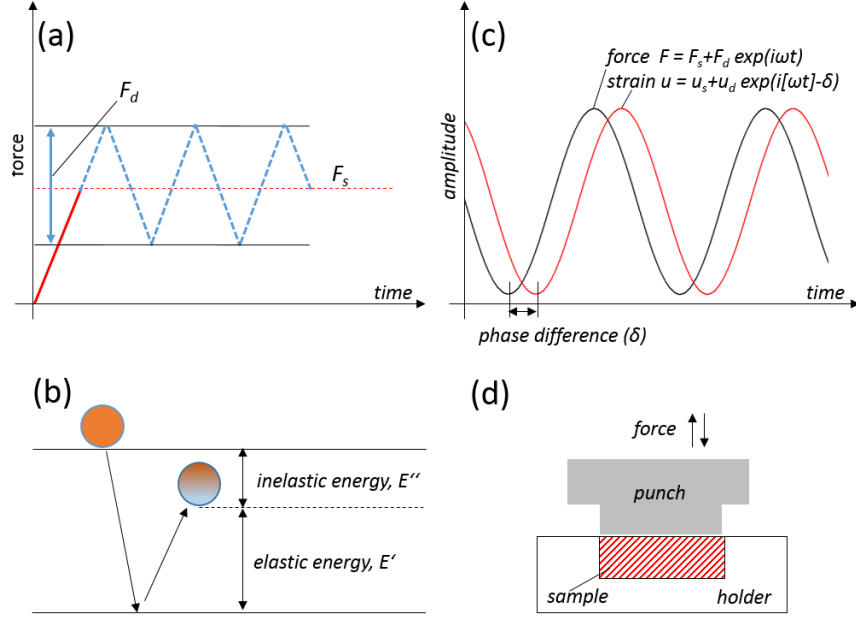
Fig. 2. Schematic illustration of DMA operation. (a) Cyclic fatigue loading including static and dynamic force components, *Fs* and *Fd*, respectively; (b) Energy losses during ball jumping (modified according to Saba et. 2016); (c) Appearance of phase shift, *δ* between the applied force *F* and the acquired strain *u* (modified from Harrison et al. 2004b); (d). Applied compression cell.

2. 3 Microstructural analysis

The microstructure of grains was examined by reflected light microscopy. For this purpose, the deformed powders were embedded in an epoxy raisin and prepared in form of thin polished sections. For the phase and microstructural analysis, X-ray powder diffraction (XRD) on Kristalloflex D500, Siemens diffractometer with a copper tube and graphite monochromator was used. Sample were scanned in the 2θ range 10-63° with an angular speed of 0.5°/min. To determine the instrumental broadening function and the exact Bragg positioning of the magnetite peaks, Si and CaWO4 powders were used as standard materials. The average lattice parameter *a*, was calculated from shifts of *Kα1* lines of (511) and (440). Apparent crystallite size was estimated from the full width at half maximum (FWHM) of the X-ray diffraction peak using Scherrer's equation:

$$D = K\lambda / (\beta \cos \theta), \tag{4}$$

where *D* is the crystallite diameter, λ the X-ray wavelength, β - the FWHM of a diffraction peak, (311) in our case, *θ* is the diffraction angle, and K is the Scherrer's constant in the order of unity for usual crystals.

Origin software (OriginPro) was used for the shape analysis of overlapped diffraction peaks.

2. 4 Magnetic properties

Susceptibility measurements around the Verwey and Curie transition temperatures were made using an AGICO KLY-4S Kappabridge at effective field intensity of 300 A/m and frequency of 875 Hz. Hysteresis loops were measured on a Princeton Measurements vibrating sample magnetometer (Institute for Rock Magnetism, Minneapolis, USA) exhibiting a sensitivity of 5 x 10^{-9} A/m². From the hysteresis loops, the values of remanent magnetization after saturation *Mrs*, saturation magnetization *Ms*, coercivity *Bc* and coercivity of remanence *Bcr* were extracted. First-order reversal curve (FORC) distributions were calculated from major hysteresis loops using FORCinel software (Harrison & Feinberg 2008). Origin software (OriginPro) was used for the analysis of coercivity distributions from backfield coercivity (BF) curves. The BF analysis was based on standard curve analysis gadgets of Origin as well as on the approach described by Maxbauer et al. (2016).

3. Results

3.1 DMA-assisted cyclic compression

Figure 3 presents the evolution in tan *δ* (ratio of loss and storage modulus or mechanical damping factor) measured as function of temperature and loading frequency. The inelastic losses occurring within the applied temperature range are proportional to the increasing loading frequency (Fig. 3a). High *tan δ* values indicate a high, non-elastic strain component while low values are indicative of higher elasticity. Until about 320°C a non-linear decrease with some irregular peaks are observed, which are likely related to water release and pre-sintering of the magnetite powder. As the studied powders exhibit relatively high specific surface areas, and therefore a high ability to absorb the atmospheric moisture, part of these non-elastic strain components can be linked to water release. Another part of the relatively strong mechanical losses up to 320°C is probably related to an energy dissipation connected with the pre-sintering, powder compaction phase. Above about 320°C, the mechanical losses are mostly attributed to the onset of irreversible inelastic losses in magnetite. Between 320 and 400°C, there is a plateau, where losses appear to be more stable. Figure 3b shows the effect of loading frequency on *tan δ* at 350°C (s. the green dashed line in Fig. 3a). The *tan δ* exhibits a non-linear behavior suggesting an anomalous behavior at 10 Hz. After DMA loadings, the compressed powders appear like well-sintered, dense bodies. Evidently, the applied incremental cyclic compression of powders forms more dense samples in analogy to the transformation of incoherent kakierite to coherent cataclasite in fault rocks. Therefore, the behavior of *tan δ* at different frequencies can be related to irreversible fatigue-induced changes in microstructural and magnetic properties of magnetite. The corresponding changes are documented in the following chapters.
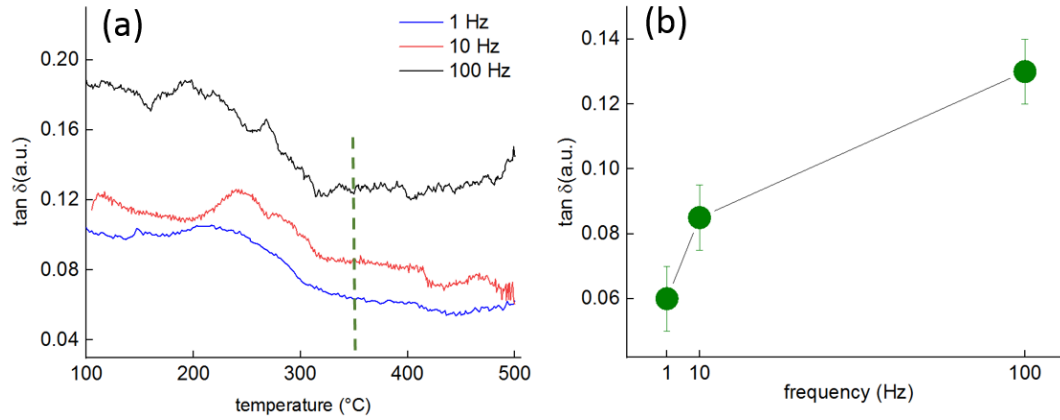
Fig. 3. Thermal and frequency dependence of tan δ (a) and the relationship between loading frequency and *tan* δ measured at 350°C (s. the green dashed line in (a)). Note the non-linear behavior in (b) indicating an increase of the non-elastic strain component at 10 Hz.

3.2 Petrographic and microstructural analysis

Figure 4 shows micrographs of polished sections of fatigued samples at different frequencies embedded in an epoxy raisin. Although preparation artifacts affecting the initial size and morphology of the grains cannot be excluded, some general trends can be recognized. In all samples tiny, about 1-2 µm thick hematite lamellae as well as quartz grains are present. After applying 1 Hz loading frequency, hematite is mainly located along edges of magnetite grains (Fig. 4a). As the loading frequency is increased to 10 Hz, a prominent fragmentation of magnetite grains in form of intragranular fractures occurs (Fig. 4b). Similar but less developed fractures occur after applying 100 Hz loading frequency (Fig. 4c). However the appearance of clearly smaller grains compared to the starting material suggests that some pulverization also occurred.
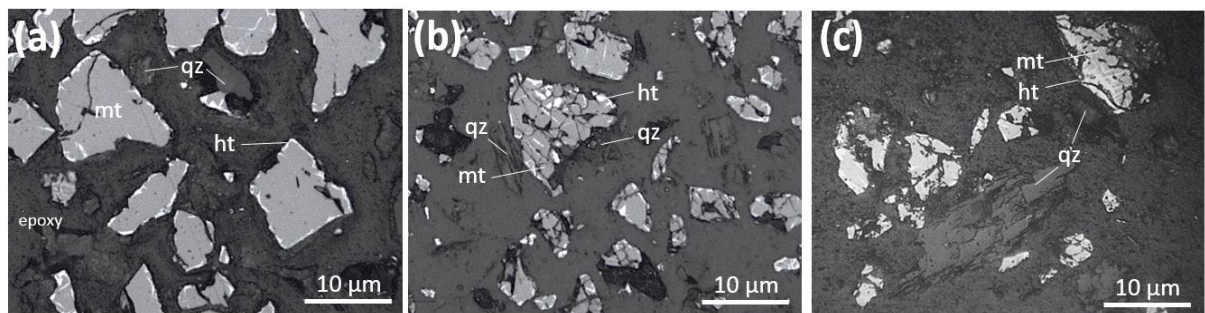

Fig. 4. Morphology of magnetite grains after applying cycling compression at 1 (a), 10 (b) and 100 Hz (c). In all samples hematite (ht) has formed due to oxidation. Note the intensive intragranular fragmentation in magnetite (mt) in the sample fatigued at 10 Hz (b), and the increased grain decohesion at 100 Hz. Reflected light micrographs from polished sections.

Figure 5 shows representative X-ray diffraction diagrams of the fatigue loaded samples. Strong magnetite and quartz peaks are typical for all studied samples. Compared to the initial sample, only the loaded samples contain the strongest (104) peak of hematite (hexagonal, R3c space group). The X-ray diffraction data correlate well with the petrographic observations showing the presence of quartz and hematite (Fig. 4). The presence of a small amount of maghemite cannot be ruled out. At low diffraction angles (Fig. 5a) the maghemite identification is extremely difficult because its peaks are overlapped with peaks of magnetite and hematite. But at high diffraction angles, there are no indications for maghemite (s. arrow in Fig. 5b)
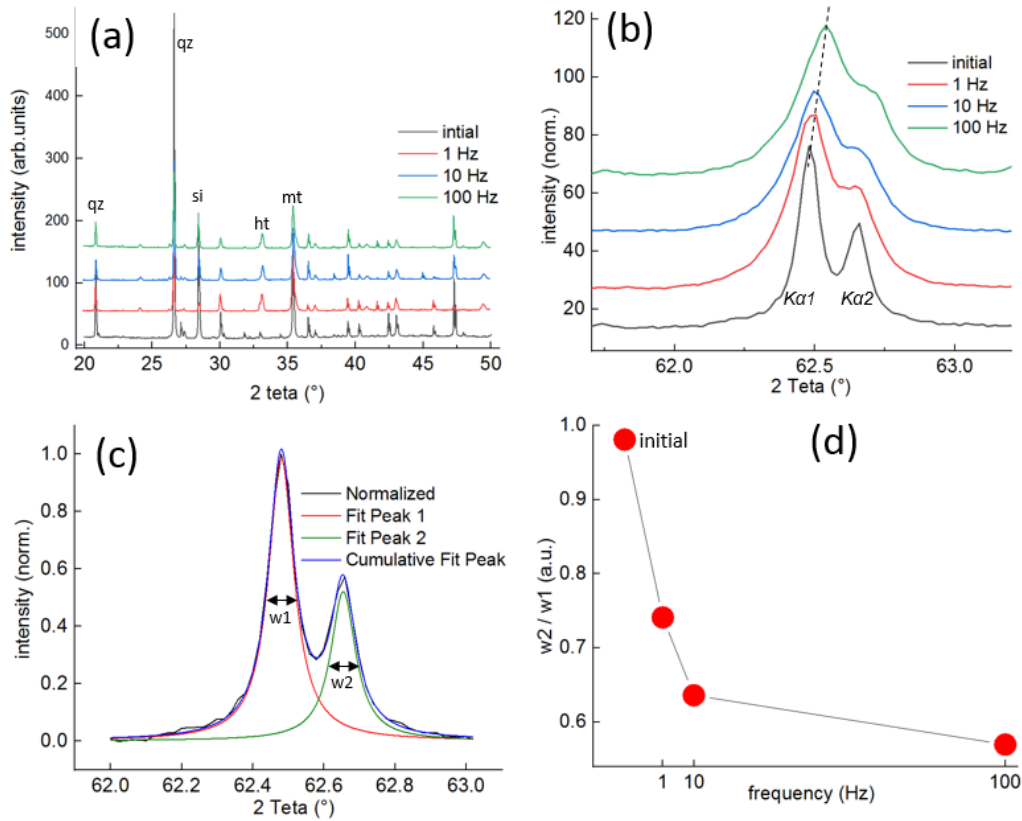

Fig. 5. Effect of loading frequency on X-ray diffraction profiles. (a) Overview diffractograms showing most intense peaks of quartz (qz), hematite (ht) magnetite (mt) and silicon (si) are labeled. The Si was used as an inner diffraction standard for measuring of apparent crystallite size and lattice constant; (b) Evolution of (440) magnetite peak composed of $K\alpha1$ and $K\alpha2$ components. Note the progressive broadening and shift (dashed line); (c) An example of doublet fitting using Lorentian function. w1 and w2 denote doublet component widths; (d) Plot of w2/w1 ratio against the loading frequency. Note the deviation at 10 Hz.

At high diffraction angles, $K\alpha1/K\alpha2$ components of the (440) magnetite peak are well-separated in the initial sample indicating a very high crystallinity degree of the non-treated magnetite (Fig. 5b). The distinct smearing of components in fatigued samples strongly indicates the presence of accumulated strains and lattice distortion in magnetite. Therefore, the peak broadening degree or the width ratio of $K\alpha1/K\alpha2$ components can likely be used as a measure of the lattice distortion degree in magnetite. For this purpose, the component widths, w1 and w2 were determined using Lorentzian

profiles (OriginPro) fitting of multiple peaks (Fig. 5c). The ratio w2/w1 appears to be sensitive to the increasing loading frequency and also suggests a deviation at 10 Hz (Fig 5d).

Figure 6 shows the effect of loading frequency on the apparent crystallite size and lattice constant. An evident reduction of the apparent crystallite size of magnetite already occurs at 1 Hz (Fig. 6a). The crystallite size of the cyclic loaded magnetite ranges between 80 and 150 nm. In addition, the lattice constant is slightly reduced with increasing loading frequency (Fig. 6b). It reaches a minimum at 100 Hz (Fig.6b), in agreement with the strongest lattice distortion, which is also indicated by the w2/w1 ratio shown in Fig. 5d.
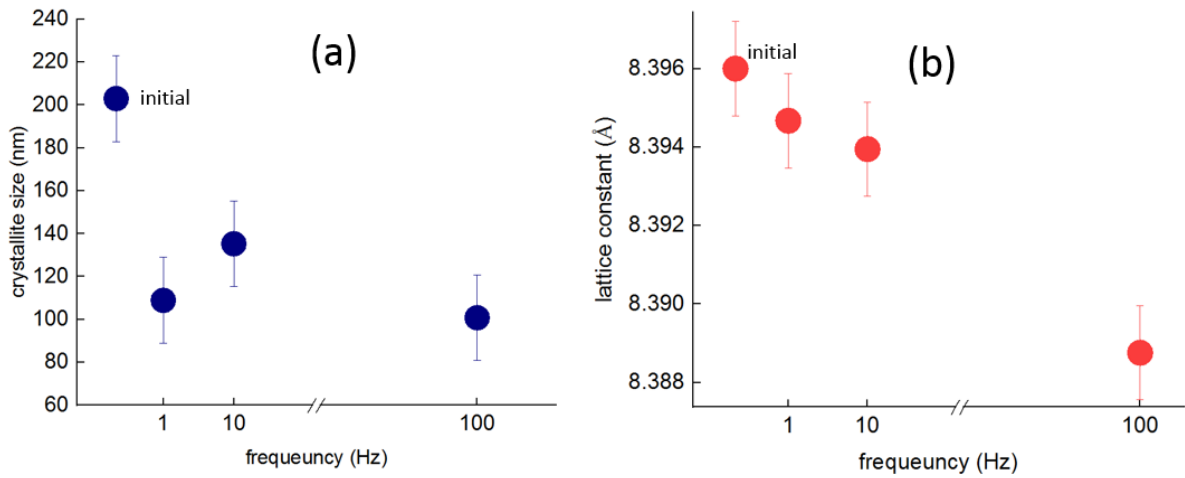

Fig. 6. Effect of loading frequency on the evolution of apparent crystallite size (a) and lattice constant (b).

3.3 Magnetic properties

3.3.1. Verwey transition

Figure 7 displays variations in magnetic susceptibility and its temperature-dependence measured across the Verwey transition towards room temperature. A strong, about 20% drop of bulk magnetic susceptibility occur at room temperature for the treated samples (Fig. 7a). Sharp Verwey transition temperature (T_V) around 120 K is observed for 1 and 100 Hz samples while for 10 Hz the transition is slightly shifted to 126 K (Fig. 7b, inset). The sharp T_V in fatigued samples clearly indicate that magnetite is the main magnetic carrier. Above T_V, the susceptibility exhibits a parabolic-shaped decay (Fig. 7b-d). Interestingly, the decay follows the Curie-Weiss law ($k\sim1/T$), which is typical for paramagnetic states although magnetite is still below its Curie temperature. There are two possible contributions influencing the drop of magnetic susceptibility in cyclic loaded magnetite: the presence of hematite and the refinement of magnetite domains. In order to understand the role of hematite on the shape and position of T_V, binary mixtures of hematite and magnetite were studied (Fig. 8a, b). As

the hematite content reaches about 10 weight percent, the bulk susceptibility starts to decrease significantly (Fig.7c). On the other hand, our results clearly document that the increasing amount of hematite (up to the here studied 70 weight %) influences only the intensity of the bulk magnetic susceptibility (Fig. 7a) but not the decayed shape of the thermomagnetic curve (Fig. 7b).
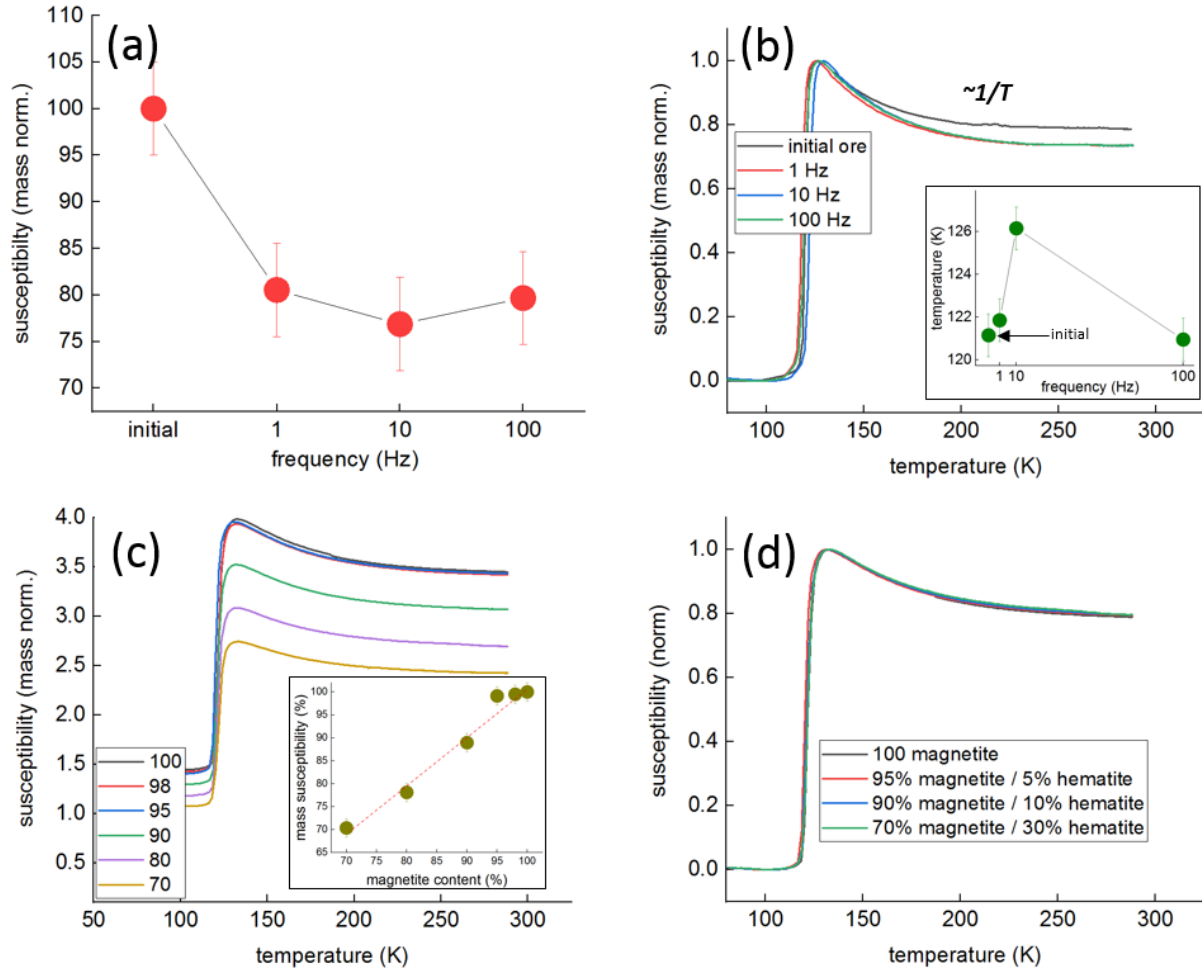

Fig. 7. Effect of loading frequency on magnetic susceptibility behavior measured across Verwey transition. (a) Depletion of bulk magnetic susceptibility at room temperature with increasing loading frequency; (b) Thermomagnetic curves exhibiting sharp Verwey transition around 121 K and an exponential drop towards room temperature; The inset shows the variation of the Verwey transition temperature as a function of loading frequency; (c) Effect of mass magnetite concentration varying from 100 to 70% on the intensity of magnetic susceptibility in magnetite-hematite binary mixtures. The inset shows the mass susceptibility versus magnetite/hematite content; (d) Effect of hematite content on the shape of the Verwey transition. For sake of clarity, only 100, 95, 90 and 80% magnetite/hematite mixtures are shown. Note that the hematite content has no effect on the shape of the total thermomagnetic curve.

We suspected that the parabolic decay above T_V (Fig. 7b) is attributed to the formation of defects in magnetite. In order to prove this hypothesis, T_V of fatigued samples were comparatively studied with

samples mechanically crushed from the initial iron ore and a single crystal magnetite. A single crystal (001) plate cut from a natural magnetite octahedron was used as a reference material. The susceptibility curve of this material exhibits nearly constant magnetic susceptibility after T_V (Fig. 8a, black curve). A significant susceptibility decay already occurs when the same sample was manually powdered (Fig. 8a red curve). Compared to the single crystal curves (Fig. 8a, black and red curves) the curve of the initial iron ore already showed a stronger decay (Fig. 8a, blue curve). The decay is getting even stronger, when the initial ore is milled (Fig. 8a, green curve). The curves of the samples cyclic loaded at different frequencies are located slightly above the curve of the powdered iron ore. To quantify the degree of magnetic susceptibility decay above T_V, the Verwey transition peak ratio, TvP according to Kontny *et al.* (2018) was calculated (Fig. 8b, inset). The TvP seems to be especially responsive to the increasing refinement degree of magnetite in powdered samples of single crystal and iron ore (Fig. 8b). Moreover, between the cyclic loaded samples, the sample loaded at 10 Hz exhibit a slightly lower TvP value. It has to be mentioned that the initial single crystal and the metamorphic iron ore are already very distinct suggesting a different original strain due to a different geological history.
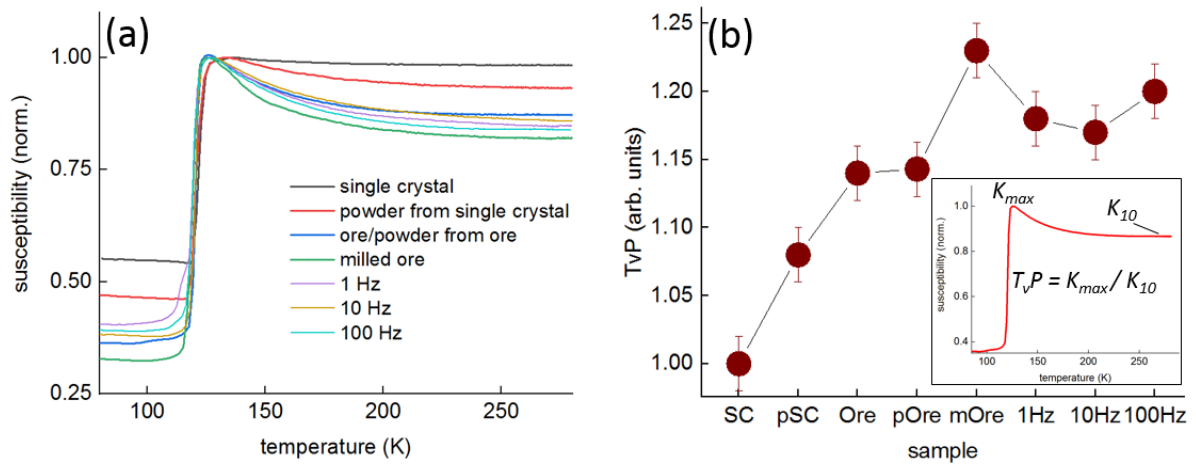

Fig. 8. Effect of the refinement degree on the shape of low-temperature thermomagnetic curves. (a) Comparison of the studied sample compressed at different loading frequencies with reference samples (s. legend and text for details). (b) Variation of the Verwey transition peak ratio (TvP). Inset: determination of the TvP according to Kontny *et al.* (2018). In (b): SC-single crystal; pSC- powder prepared by manual grinding from single crystal; Ore- initial ore; pOre-powder prepared from ore manual grinding; mOre- milled powder prepared from ore by achate mill; 1, 10 and 100 Hz -cyclic loaded ore samples.

3.3.2 Hysteresis behavior

The results of the hysteresis measurements are presented in Fig. 9. Hysteresis loops of all samples (Fig. 9a) exhibit typical S shapes which are typical for MD magnetite. Some differences become obvious when plotting *Mrs/Ms* versus *Bcr/Bc* in a Day-Dunlop diagram (Dunlop 2002) indicating a small change in magnetic domain size from the field of multi domain (MD) into the field

of pseudo single domain (PSD) behavior (Fig. 9b). The increase in Bc, Bcr (Fig. 9c) as well in Ms and Mrs (Fig. 9d) also suggests the increasing portion of PSD domains (Fig. 9b) is controlled by the loading frequency. The abrupt drop of Ms from 71.37 Am^2/kg in the initial magnetite to values around 56 Am^2/kg in the 1 Hz sample is likely partly related to the formation of hematite.
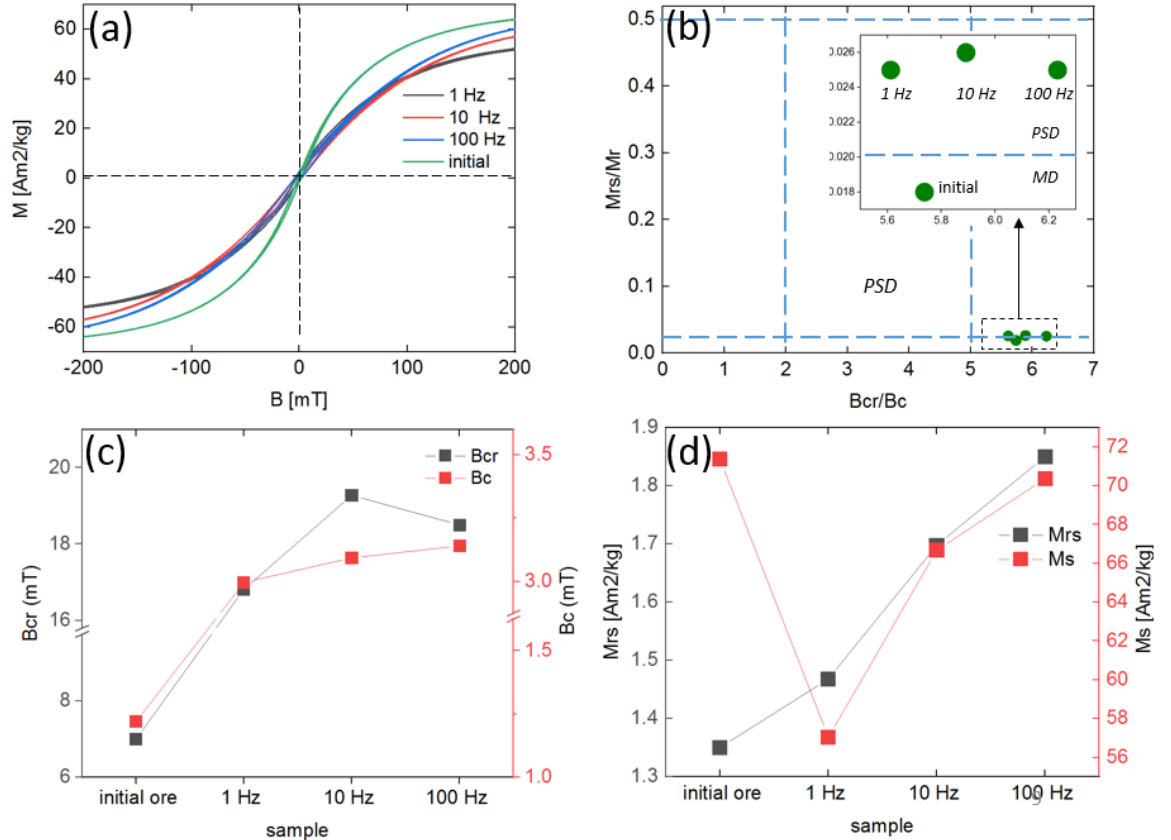

Fig. 9. Effect of cyclic loading on the hysteresis behavior. (a) Magnetic hysteresis loops; (b) Day-Dunlop plot of ratios of hysteresis parameters (Dunlop 2002) with the inset suggesting domain refinement in cyclic-loaded magnetite from the MD to the PSD field; (c) Coercivity parameters Bcr and Bc as a function of the loading frequency; (d) Remanence parameters Mr and Mrs as a function of the loading frequency.

FORC distributions shown in Fig. 10 compare the fatigued samples (middle row) with samples prepared from the initial ore (top row) and with sample mixtures containing hematite (bottom row). With exception of FORC from hematite, a well-developed maximum at about 0.015 T occurs in all, also the cyclic loaded samples indicating that soft-magnetic magnetite is the main magnetic carrier. The diagrams of the powders prepared by manual grinding and by achate mill (corresponds to values of 100% magnetite or "powder from milled ore" in magnetite-hematite mixtures shown in Fig. 8) are characterized by an increasing spread along the horizontal axis (s. the red arrows) towards higher coercivity as well as by the growing area labelled as red hillocks. This type of FORC distributions is representative MD-PSD mixtures (Harrison & Feinberg 2008, Reznik *et al.* 2016). Furtermore, the evolution trend of FORC diagrams of the powders prepared from the ore is in a good accordance with behavior of the TvP ratio which is growing with increasing refinement of magnetite (Fig.8). The FORCs of fatigued sample appear to be very similar to the FORC diagram of powders prepared

manually from the initial ore while the hereditary traits in milled ore can be recognized in binary hematite-magnetite mixtures containing 5 and 10 % of milled magnetite (Fig. 10, bottom row).
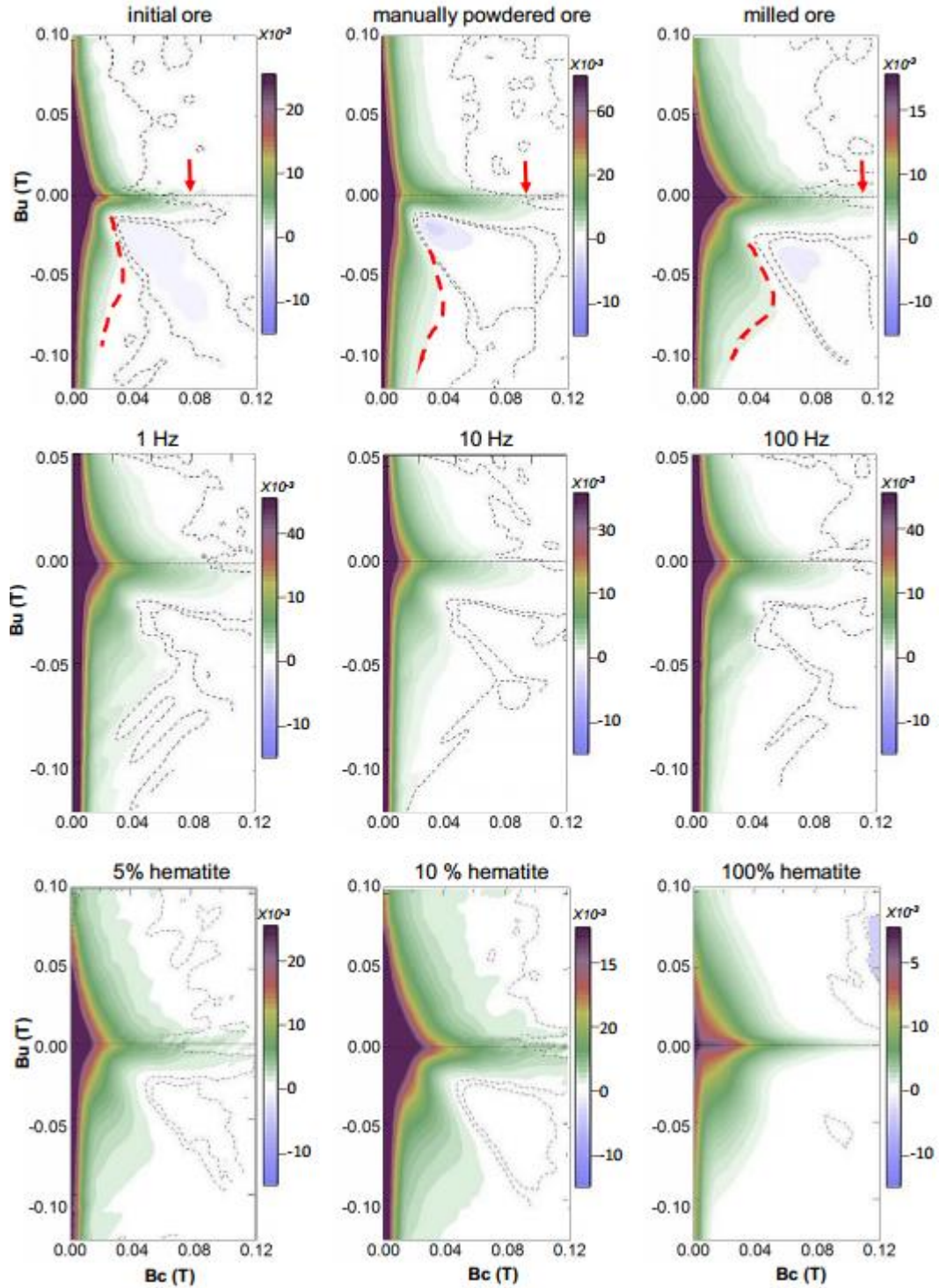

Fig. 10 FORC diagrams of the studied samples. Note the extended broadening of signals in cyclic loaded samples indicating the presence of MD-PSD mixtures. The blue arrows and the red humps illustrate the increasing intensity of signals related to mechanically induced defects.

The recorded FORC distributions exhibit a good potential in recognizing of the mechanically induced refinement in magnetite. However, FORC distributions, as well as hysteresis behavior, appear to be non-sensitive to the presence of hematite in fatigued samples. To estimate the proportion of different magnetic components, deconvolution or unmixing of BF curves have been carry out.

Figure 11 demonstrates results of magnetic component analysis performed with Origin-Software deconvolution procedure using Gaussian functions. A typical BF curve of a fatigued sample exhibits an asymmetric shape (Fig. 11a, black squares) and shows no signals around 2.3 mT which are characteristic for hematite (Maxbauer et al. 2016). After the deconvolution procedure, the curve is presented as sum of two components: a broad component 1 (green curve) and a sharp component 2 (blue curve). The shape and position of the curve of the component 1 approaches those of the initial ore (red curve) as well as of the single crystal magnetite (not shown here). The shape and position of the curve of component 2 approaches curve behavior of the milled ore (blue curve). Figure 11b-c are plots illustrating the relationship between the loading frequency and some components parameters Remarkably, all parameters exhibit a non-linear relationship with increasing loading frequency and display a deviation at 10 Hz corresponding to the highest (about 65%) of PSD grains (Fig.11d).
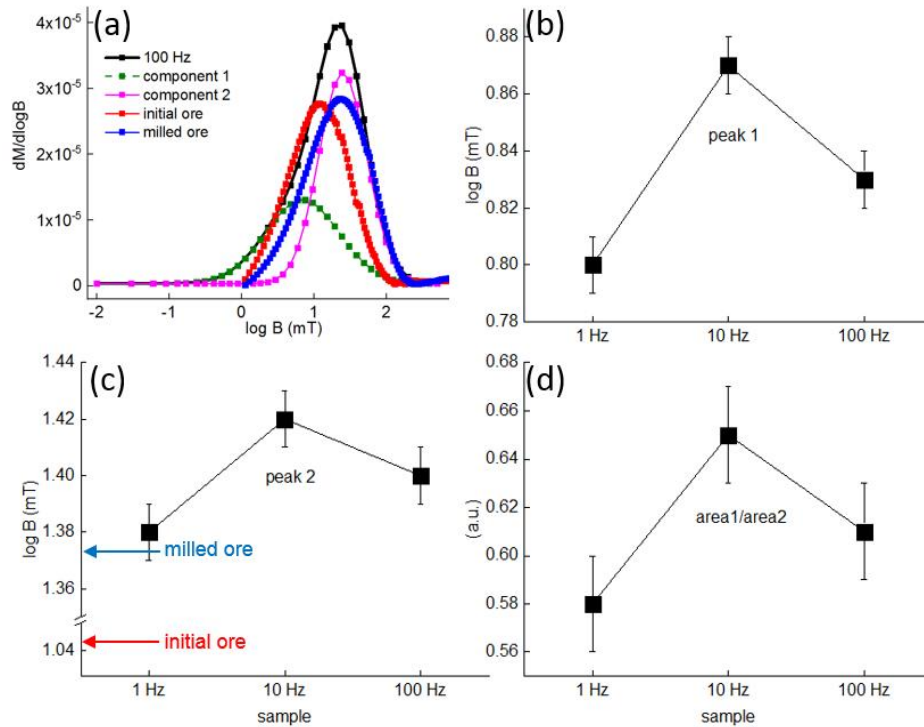

Fig. 11. Coercivity parameters derived from BF measurements. (a) An example showing that the asymmetric curve (black quadrats) of a fatigued sample (shown for 100 Hz sample) consists of two symmetric curves - curve of component 1 (green curve) and curve of component 2 (magenta curve). For comparison, the symmetric curves of initial (blue curve) and milled ore (red curve) are also shown; (b-d) Parameters as a function of the loading frequency. Note the deviation at 10 Hz.

4. Discussion

We present for the first time results demonstrating the relationship between cyclic, seismic-related laboratory compression as a function of loading frequencies and magnetic properties of MD magnetite. Table 1 compares some parameters obtained by the combination of magnetic and non-magnetic, microstructure-sensitive methods and indicates the relationship between the mechanical loss, lattice distortion, crystallite or grain size reduction, and magnetite oxidation.

Table 1. Effect of the loading frequency on the alteration of structural and magnetic parameters.

$\tan \delta$: DMA mass loss measured at 350°C; w2/w1: width ratio measured by XRD; d: crystallite size measured by XRD; χ: bulk magnetic susceptibility; Tv: Verwey transition temperature; TvP: Verwey transition peak ratio; Ms: saturation magnetization; Mrs: magnetic remanence; Bc: coercivity; Bcr: back field coercivity; area 1/area 2: magnetic component ratio extracted from BF curves. Red numbers highlight anomalous deviations at 10 Hz loading.

parameter	unit	initial	1 Hz	10 Hz	100 Hz	indication
tan δ	a.u.		0.003	0.085	0.13	mechanical loss
w2/w1	a.u.	0.98	0.74	0.63	0.56	lattice distortion
d	nm	210	110	128	105	apparent crystallite reduction
χ	10-6(m3/kg)	1.27	1.01	0.92	0.87	oxidation and grain reduction
Tv	K	121	122	126	121	lattice distortion
TvP	a.u.	1.14	1.19	1.16	2	grain reduction
Ms	Am2/kg	71.37	57.03	66.67	70.36	oxidation
Mrs	Am2/kg	1.35	1.47	1.7	1.85	grain reduction
Bc	mT	1.22	3	3.09	3.14	grain reduction
Bcr	mT	7	16.80	19.28	17.40	grain reduction
Bcr/Bc	a.u.	5.74	5.61	6.23	5.9	grain reduction
Mr/Ms	a.u.	0.018	0.025	0.026	0.025	grain reduction
area1/area2	a.u		0.58	0.65	0.61	MD/PSD-mixture

4.1 Mechanical losses vs magnetic and structural properties

Magnetite-quartz ore powders were cyclic deformed at a static force of 6 MPa and a modulated force of 3 MPa from room temperature to 500 °C in ambient atmosphere. Even if this static pressure was significantly below the Young´s modulus of magnetite lying around 200 GPa (Doraiswami 1947), notable mechanical losses indicated by *tan δ* (phase lag between applied stress and resultant strain) take place at all loading frequencies. The mechanical loss shows a non-linear behavior between 1 and 100 Hz (Table 1, Fig. 3). The cyclic loading at different frequencies produced different degrees of fragmentation, but all in common is an oxidation of magnetite into hematite along grain boundaries and preferred lattice orientations (Fig. 4). The microscopic observations rather suggest that oxidation occurred before fracturing. The mechanical loss seems to be directly related to the degree of fragmentation and lattice distortion (compare Fig. 3b with Fig. 5d) and is in magnetic

properties best reflected in the T_VP value (compare Fig. 3b with Fig. 8b), but also in all other magnetic properties (Table 1).

The evolution of mechanical losses suggests an anomaly at 10 Hz (Fig. 3b, Table 1). This loading frequency is characterized by the strongest intra-crystalline fragmentation in magnetite (Fig. 4b), crystallite refinement and lattice distortion as retrieved from XRD peaks (Fig. 6a, Table 1). The anomaly at 10 Hz has been observed independently by different structure-sensitive and magnetic methods and signifies the non-linear dynamic deformation. As the used loading frequencies correspond to generally registered frequencies under which strong earthquake hazards occur (Fig. 1), the revealed net of relationships (Table 1) propose a powerful petrophysical tool for studying seismic-related failures.

4.2 Magnetic response to fatigue compression

All applied magnetic methods display a good sensitivity to the loading frequency (Table 1, Figs 9-11.), but our results also show that under the applied fatigue loading conditions two competing mechanisms occur. The first is the magnetic fatigue, that is related to grain fragmentation and defect structures in the magnetite lattice, the second is related to the oxidation of magnetite into hematite (Figs 4, 5a). Therefore, we have to distinguish between these two mechanisms, and we have to be sure which magnetic property changes are sensitive to magnetite deformation and which are affected by the magnetite/hematite ratio.

The separation of features related to hematite from those related to magnetite is not straightforward from magnetic methods alone. Ahmadzadeh et al. (2018) studied similar binary hematite-magnetite mixtures as we have done in this study, and noted that the magnetic signals from hematite can be easily muted when magnetite content is higher than 5 wt%. According to Liu *et al.* (2019) hysteresis parameters only vary significantly from pure magnetite if in the hematite-magnetite mixtures the hematite concentrations is higher than 90 wt%. In FORC diagrams, hematite is also only visible in concentrations >30 wt%. The main reason for this behavior is that magnetite exhibits high magnetization (~92 Am2/kg) and low coercivity (10-40 mT) while hematite displays small magnetization (~0.4 Am2/kg) and high coercivity (~100-400 mT) (Ahmadzadeh *et al.* 2018).

The most evident magnetic properties indicating hematite in our study are the magnetic susceptibility (χ) and the magnetization (*Ms*) because they decrease due to the dilution effect of hematite (Table 1). According to our magnetic susceptibility measurements of magnetite-hematite mixtures (Fig.7c, inset) the hematite concentration in our loaded samples should be around 17% for the 1 and 10 Hz samples and about 20% for the 100 Hz sample. Compared to the microscopic observations this seems to be quite high (Fig. 4). Remarkably, a very similar drop in magnetic susceptibility was also observed in experimentally shocked samples originating from the same magnetite-quartz ore, where we identified no traces of hematite (Reznik. *et al.* 2016) or maghemite

(Kontny *et al.* 2018). Therefore, mechanical refinement of magnetite also causes a significant drop in magnetic susceptibility and part of the magnetic susceptibility drop in the cyclic loaded magnetite is clearly related to lattice distortion and grain size refinement (Fig.5).

The evolution of hysteresis behavior proves the fatigue-induced refinement. Mr and Bcr are especially sensitive to the increasing loading frequency (Table 1). The drop in Ms observed at 1 Hz indicate a strong dilution with hematite in this sample (Fig. 11d, red symbols). According to the Day-Dunlop plot (Fig. 9b, Table1), the fatigued samples are shifted towards the PSD field of magnetite. The FORC distributions of the fatigued samples contain no coercivity signals lying above 60 mT (Fig.10, middle row) and appear like MD-PSD mixtures in magnetite (see e.g. Roberts et al. 2000, Reznik et al. 2016), and are similar to the FORC diagrams of powders prepared from the initial ore (Fig.10, top row). Furthermore, the presence of MD-PSD mixtures in fatigues samples is also confirmed by the coercivity distributions (Fig. 11, Table 1) showing two soft components. Interestingly, the coercivity of component 2 (Fig. 11a, black circles) lies near the coercivity values reported by Maxbauer et al. (2017) for pedogenic magnetite exhibiting magnetic behavior of superparamagnetic(<30 nm) or stable-single domain (30-75 nm) grains. This would rather indicate mixtures over a larger coercivity spectra. The apparent crystallite size of cyclic loaded magnetite for all frequencies are in the range between 80 and 150 nm (Fig. 6a).

Comparing the synthetic hematite with our cyclic loaded samples, the µm-sized particles of synthetic hematite produce a big number of diffraction peaks indicating a very high degree of crystallinity. In FORC diagrams this material displays MD magnetic behavior (s. FORC diagram of 100% hematite in Fig. 10). The submicron-sized grains of hematite from the cyclic loaded samples show a very low degree of crystallinity (Fig. 5a) and therefore should display properties of relatively hard magnetic particles. The FORC diagrams presented in this study clearly show that the hematite cannot be discriminated from cyclic loaded magnetite because milled magnetite powder (magnetic domain refinement), cyclic loaded samples (magnetic domain refinement and hematite) and hematite-magnetite mixtures show very similar distributions of B_u and B_c.

The behavior of magnetic susceptibility across the Verwey transition towards room temperature (*TvP)* also appears to be sensitive to magnetic fatigue and we have shown that the parabolic-shaped decay above *Tv* is totally independent of hematite admixture (Fig. 7c, d). We demonstrated that an amount of hematite up to 30 wt % has no influence on the transition temperature (Fig. 7c, d) in agreement with other studies (e.g. Ahmadzadeh *et al.* 2018, Liu *et al.* 2019) . At the same time, *Tv* for initial magnetite and cyclic loaded samples at 1 and 100 Hz is the same, indicating that magnetite has not changed, e.g. oxidized to maghemite. In the 10 Hz sample a slightly higher *Tv* was measured (Fig. 7b, inset, Table 1). According to Aragón *et al.* (1985), cation vacancies due to oxidation in magnetite would reduce *Tv*. Therefore we suspect that the small increase in Tv might indicate a higher amount of strain (e.g. Carporzen & Gilder 2010, Reznik et al. 2016). Our data clearly

demonstrate that the decay above *Tv* is related to (1) lattice strain and (2) crystallite and magnetic grain size. Powders from magnetite single crystals or from the magnetite ore always show a stronger decay than the starting material (Fig. 8). Therefore, the changes in *TvP* ratio (see inset in Fig. 8b, Table 1) in the cyclic loaded samples can be mainly attributed to the formation of fatigue induced defects in magnetite. Interestingly, a very similar decay was observed in *TvP* of experimentally shocked magnetite ore (Reznik. *et al.* 2016) confirming the significance of lattice strain and magnetic domain size reduction. A numerical procedure modelling the effect of the refinement degree on the shape of *TvP* is presented in an ongoing work (Fuchs *et al.* 2019). In this context it is interesting to note that magnetic moments of surface atoms in magnetite decrease due to point defects at the grain surface (Noh *et al.* 2015). From experiments, the defects created by mechanical treatment in some minerals are known as stable paramagnetic centers (e.g. Maniatis & Mandi 1992, Caurant et al. 1995). Therefore, the parabolic susceptibility decay (Fig. 7b-d, Fig. 8) can be associated with paramagnetic defects located at the surfaces of intragranular cracks and grain boundaries of the fatigued magnetite grains. Evidently, the loading at 10 Hz is more favorable for brittle deformation and enhanced defect density (see *TvP* value in Table 1).

Fracturing can form new grain boundaries (Fig. 4) with fresh surfaces acting as growth centers for hematite. For example, vacancies, formed primarily on the magnetite surfaces, are described to play a significant role for the oxidation of magnetite. Nie et al. (Nie *et al.* 2013) described two spatially separated reactions for the magnetite oxidation:

$$2O_2 + 6e^- \longrightarrow Fe_3O_4 + 3V_{Fe}^{\ 2-} \tag{5}$$

$$3\ Fe_3O_4 + V_{Fe}^{\ 2-} \longrightarrow 4Fe_3O_4 + 2e^- \tag{6}$$

The localization of hematite at magnetite grain boundaries might suggest that dissolution creep mechanisms like movement of vacancies and interstitials along cleavage planes and grain boundaries favor its formation (see e.g. Noh *et al.* 2015). This interpretation is in agreement with the postulated dissolution creep deformation in magnetite below 500°C according to the deformation map given in Till & Moskowitz (2013). Hence, the hematite localizes primary at magnetite grain boundaries while the interiors are mostly free of hematite (Fig. 4). We have no XRD or magnetic indications that this reaction goes via maghemite in our cyclic loaded samples.

Actually, we do not have any indication for a stronger hematite formation along fresh surfaces and indeed it likely looks like that oxidation occurs prior to fracturing in our samples (Fig. 4). Therefore, we observe a two-stage mechanism with (1) oxidation of magnetite in ambient atmosphere, and (2) magnetic fatigue in magnetite. In this study we have not seen that a catalytic cycle of magnetite oxidation to hematite is closely related to the cyclic deformation history in our magnetite. The hematite concentration has not increased due to cyclic loading frequency. It can be speculated that this observation indicates the formation of a core (magnetite) - shell (hematite) structure where

the hematite shell acts as a passivation layer reducing chemical activity of magnetite and protecting simultaneously its core from further oxidation.

5. Conclusions

Powders of multidomain magnetite were subjected to laboratory seismic-related loading at ambient conditions using cyclic compression at 6+3 MPa in the temperature range between 30 and 500°C. The properties of fatigued powders were subsequently studied as a function of the loading frequency by a combination of microstructural and magnetic methods, and the following results are obtained:

- Although the applied static pressure was only 6 MPa, which is significantly below the Young´s modulus of magnetite (about 200 GPa) at all applied loading frequencies, there are visible changes in mechanical loss and in magnetic and microstructural properties.

- Under applied fatigue compressions, magnetic fatigue in magnetite is accompanied by hematite formation (mineral reaction).

- Magnetic fatigue is related to internal friction in magnetite and is characterized by grain crushing, refinement of magnetic domains and formation of lattice defects.

- The degree of susceptibility decay above Verwey transition, *TvP*-ratio is a sensitive fingerprint of magnetic fatigue.

- Hysteresis properties are sensitive to defects produced by fatigue loading. However, the signals related to hematite cannot be easily extracted because they are masked by much stronger signals of magnetite. Thus, the magnetic data should be validated by microstructural sensitive method like microscopy or XRD.

- Both, magnetic and non-magnetic properties reveal a characteristic resonance at 10 Hz corresponding to the seismic frequency at which the biggest damages produced by earthquakes are established.

We have shown in this study that during dynamic mechanical analyses low static forces of 6 MPa modulated with 3 MPa are sufficient to cause magnetic fatigue in magnetite, and we have demonstrated which mechanisms are mainly responsible for magnetic and microstructural changes. Further seismic-related loading experiments in a broader range of conditions are in progress on rock plates in order to verify and elaborate the mechanisms shown in this study on magnetite powders.

References

Ahmadzadeh, M., Romero, C. & McCloy, J. (2018) Magnetic analysis of commercial hematite, magnetite, and their mixtures. *AIP Adv.*, **8**. doi:10.1063/1.5006474

Aragón, R., Buttrey, D.J., Shepherd, J.P. & Honig, J. (1985) Influence of nonstoichiometry on the Verwey transition. *Phys. Rev. B*, **31**, 430–436.

Braunagel, M.J. & Griffith, W.A. (2019) The Effect of Dynamic Stress Cycling on the Compressive Strength of Rocks. *Geophys. Res. Lett.*, **46**, 6479–6486. doi:10.1029/2019GL082723

Carporzen, L. & Gilder, S.A. (2010) Strain memory of the Verwey transition. *J. Geophys. Res. Solid Earth*, **115**, 1–12. doi:10.1029/2009JB006813

Caurant, D., Gourier, D., Demoncy, N., Ronot, I. & Pham-Thi, M. (1995) Paramagnetic defects induced by mechanical stress in calcium sulfide phosphor. *J. Appl. Phys.*, **78**, 876–892. doi:10.1063/1.360278

Cerfontaine, B. & Collin, F. (2018) Cyclic and Fatigue Behaviour of Rock Materials: Review, Interpretation and Research Perspectives. *Rock Mech. Rock Eng.*, **51**, 391–414, Springer Vienna. doi:10.1007/s00603-017-1337-5

Doraiswami, M. (1947) Elastic constants of magnetite, pyrite and chromite. *Proc. Math. Sci.*, 413–416.

Dunlop, D.J. (2002) Theory and application of the Day plot (Mrs/Ms versus Hcr/Hc) 2. Application to data for rocks, sediments, and soils. *J. Geophys. Res.*, **107**, 2057. doi:10.1029/2001JB000487

Fuchs, H., Reznik, B., Schilling, F. & Kontny, A. (2019) Evaluation of temperature-dependent magnetic susceptibility curves around the Verwey transition: insights into the deformation history of magnetite. *AGU Fall Meet. San-Francisco, USA*.

Gomberg, J. & Johnson, P. (2005) Dynamic triggering of earthquakes. *Nature*, **437**, 830–830. doi:10.1038/nature04167

Harrison, R.J. & Feinberg, J.M. (2008) FORCinel: An improved algorithm for calculating first-order reversal curve distributions using locally weighted regression smoothing. *Geochemistry, Geophys. Geosystems*, **9**. doi:10.1029/2008GC001987

Harrison, R.J., Redfern, S.A.T., Buckley, A. & Salje, E.K.H. (2004) Application of real-time, stroboscopic x-ray diffraction with dynamical mechanical analysis to characterize the motion of ferroelastic domain walls. *J. Appl. Phys.*, **95**, 1706–1717. doi:10.1063/1.1639949

Klumbach, S. & Schilling, F.R. (2013) Elastic and anelastic properties of a- and b-quartz single crystals. *Eur. J. Miner.* doi:10.1127/0935-1221/2014/0026-2362

Kontny, A., Reznik, B., Boubnov, A., Göttlicher, J. & Steininger, R. (2018) Postshock Thermally

Induced Transformations in Experimentally Shocked Magnetite. *Geochemistry, Geophys. Geosystems*, **19**, 921–931. doi:10.1002/2017GC007331

Liu, P., Hirt, A.M., Schüler, D., Uebe, R., Zhu, P., Liu, T. & Zhang, H. (2019) Numerical unmixing of weakly and strongly magnetic minerals: Examples with synthetic mixtures of magnetite and hematite. *Geophys. J. Int.*, **217**, 280–287. doi:10.1093/gji/ggz022

Maniatis, Y. & Mandi, V. (1992) Electron-paramagnetic-resonance signals and effects in marble induced by working. *J. Appl. Phys.*, **71**, 4859–4867. doi:10.1063/1.350630

Martin, R.J., Habermann, R.E. & Wyss, M. (1978) The effect of stress cycling and inelastic volumetric strain on remanent magnetization. *J. Geophys. Reasearch*, **83**, 3485–3496.

Maxbauer, D.P., Feinberg, J.M. & Fox, D.L. (2016) MAX UnMix: A web application for unmixing magnetic coercivity distributions. *Comput. Geosci.*, **95**, 140–145, Elsevier. doi:10.1016/j.cageo.2016.07.009

Maxbauer, D.P., Feinberg, J.M., Fox, D.L. & Nater, E.A. (2017) Response of pedogenic magnetite to changing vegetation in soils developed under uniform climate, topography, and parent material. *Sci. Rep.*, **7**, 1–10, Springer US. doi:10.1038/s41598-017-17722-2

Nagata, T. (1961) *Rock magnetism*, Tokyo: Maruzen Company LTD.

Nagata, T. & Kinoshita, H. (1964) Effect of release of compression on magnetization of rocks and assemblies of magnetic minerals. *Nature*, **204**, 1183–1184.

Nie, S., Starodub, E., Monti, M., Siegler, D., Vergara, L., Gabaly, F. El, Bartelt, N., *et al.* (2013) Insight into Magnetite's Redox Catalysis from Observing Surface Morphology during Oxidation. *J. Am. Chem. Soc.*, **135**, 10091–10098.

Noh, J., Osman, O.I., Aziz, S.G., Winget, P. & Brédas, J.L. (2015) Magnetite Fe3O4 (111) Surfaces: Impact of Defects on Structure, Stability, and Electronic Properties. *Chem. Mater.*, **27**, 5856–5867. doi:10.1021/acs.chemmater.5b02885

Origin(Pro). (n.d.) OriginLab Corporation *Version*.

Peng, Z. & Redfern, S.A.T. (2013) Mechanical properties of quartz at the ??-?? Phase transition: Implications for tectonic and seismic anomalies. *Geochemistry, Geophys. Geosystems*, **14**, 18–28. doi:10.1029/2012GC004482

Reznik, B., Kontny, A., Fritz, J. & Gerhards, U. (2016) Shock-induced deformation phenomena in magnetite and their consequences on magnetic properties. *Geochemistry, Geophys. Geosystems*, **17**, 2374–2393. doi:10.1002/2016GC006338.Received

Roberts, A.P., Pike, C.R. & Verosub, K.L. (2000) First-order reversal curve diagrams: A new tool for characterizing the magnetic properties of natural samples. *J. Geophys. Res. Solid Earth*, **105**, 28461–28475. doi:10.1029/2000jb900326

Saba, N., Jawaid, M., Alothman, O.Y. & Paridah, M.T. (2016) A review on dynamic mechanical properties of natural fibre reinforced polymer composites. *Constr. Build. Mater.*, **106**, 149–159, Elsevier Ltd. doi:10.1016/j.conbuildmat.2015.12.075

Till, J.L. & Moskowitz, B. (2013) Magnetite deformation mechanism maps for better prediction of strain partitioning. *Geophys. Res. Lett.*, **40**, 697–702. doi:10.1002/grl.50170

Till, J.L., Moskowitz, B.M. & Jackson, M.J. (2012) High-temperature magnetic fabric development from plastically deformed magnetite in experimental shear zones. *Geophys. J. Int.*, **189**, 229–239. doi:10.1111/j.1365-246X.2011.05338.x

Volk, M.W.R. & Feinberg, J.M. (2019) Domain State and Temperature Dependence of Pressure Remanent Magnetization in Synthetic Magnetite: Implications for Crustal Remagnetization. *Geochemistry, Geophys. Geosystems*, **20**, 2473–2483. doi:10.1029/2019GC008238